BNAM 2026
Baltic-Nordic Acoustics Meeting
May 04-06 2026 Gothenburg, Sweden

Characterizing Wind Turbine Acoustic Emissions at WiValdi: A Field Study on Directional Sound Propagation and Amplitude Modulation

Shy-Yea Lin*, Alexandre Suryadi, Philipp Seelemeyer, Nan Hu and Michaela Herr

Institute of Aerodynamics and Flow Technology, German Aerospace Center (DLR), Lilienthalplatz 7 38108 Braunschweig, Germany

*shy-yea.lin@dlr.de

This paper presents a one-month unsupervised acoustic field campaign conducted at WiValdi, a research wind farm in Krummendeich, Germany. A single permanent sound monitoring station was deployed at distances of 2 and 6.4 rotor diameters from two modern multi-megawatt wind turbines, enabling directional analysis of sound propagation and revealing clear amplitude modulation (AM) patterns linked to the blade passage frequency (BPF). In order to isolate turbine-generated sounds from ambient noise, an advanced data filtering approach was applied, combining statistical descriptors, wind speed thresholds, and AM prominence criteria. The filtered dataset exhibits strong agreement with high-signal-to-noise reference measurements from a concurrent short-term emission campaign, validating the effectiveness of the proposed methodology. This study demonstrates the feasibility of using a single monitoring station in an open field, when supported by a robust data filtering approach, can reliably infer directional sound characteristics and AM patterns under real-world conditions, despite inherent limitations in noise immunity and spatial resolution. A follow-up study is underway, deploying a multi-station array at WiValdi to enable high-fidelity mapping of sound directivity, quantification of propagation effects, and validation of low-noise blade designs. These efforts will strengthen the scientific foundation for assessing AM in wind turbine noise and support the development of more robust, standardized measurement protocols for future regulatory frameworks.

1 Introduction

Wind energy plays a pivotal role in the global transition towards carbon neutrality, yet noise immission from wind turbines remains a significant barrier to public acceptance, influencing permitting processes, community engagement, and project feasibility. While substantial progress has been made in modelling turbine sound sources—particularly airfoil self-noise—the accurate prediction of sound immission under real-world, variable meteorological conditions remains a major challenge [1, 2, 3, 4]. Standardized emission measurements, such as those defined in IEC 61400-11:2012 [5], are typically short-term and conducted under high-signal-to-noise ratio (SNR) conditions, making them suitable for certification purposes but insufficient for capturing dynamic influence of atmospheric effects such as wind shear, temperature gradients, and turbulence.

Long-term sound immission monitoring offers a more realistic assessment of noise propagation across complex landscapes. However, such measurements are frequently compromised by ambient noise—such as wind-induced microphone noise, vegetation rustling, and distant traffic—leading to low SNR. Crucially, turbine-off background measurements, essential for noise filtering and spectral subtraction, are rarely available, as wind park operators typically avoid shutdowns to maintain energy production and operational continuity. This limits the applicability of conventional filtering techniques and underscores the need for robust, data-driven methods capable of identifying turbine-generated sound immission with minimal ambient noise influence—without relying on turbine-off data.

Furthermore, there remains a notable lack of direct validation of sound emission predictions against field measurements under variable atmospheric conditions. While some studies [6, 7, 8] have explored nocturnal or directional effects, they are often limited in duration or spatial coverage. To address these gaps, this study presents a novel data filtering procedure for long-term immission monitoring, enabling the identification of high-quality turbine sound segments based on signal characteristics and environmental conditions. These selected data are validated against high-fidelity, short-term emission measurements obtained during a concurrent campaign using a hemisphere-based propagation model. This dual-campaign approach allows for a direct, qualitative assessment of sound propagation under real-world conditions, advancing the scientific foundation for noise prediction, regulatory frameworks, and public trust in wind energy.

The remainder of this paper is structured as follows: Section 2 describes the WiValdi Research Wind Farm and the design of the two complementary field measurement campaigns. Section 3 details the proposed data filtering procedure. Section 4 presents the results, including the performance of the selection method, the validation framework and the observed propagation patterns. Section 5 discusses the implications, draws conclusions, and outlines future research directions.

2 Field Measurement Setup

2.1 WiValdi Wind Farm Overview

The WiValdi research wind farm is located in Krummendeich, Germany, and hosts two identical multi-megawatt wind turbines: OPUS 1 and OPUS 2. Each turbine has a rotor diameter $D = 116$ m and hub height $H = 92$ m. The turbines are separated by 4.4D, with OPUS 2 located east-northeast of OPUS 1. A meteorological mast (Mast 1) is installed 2D west-southwest of OPUS 1, aligned with the turbine axis. The site features flat terrain with plowed fields and residual corn stalks (height < 20 cm), resulting in variable ground impedance. Soil conditions varied diurnally: soft during the day and frozen at night during the period of the measurement campaign, potentially influencing ground reflection and sound propagation.

A dense array of sensors is instrumented on Mast 1 and the wind turbines. For this study, data from the following systems are used:

- Turbine operational parameters (rotor speed, power output, status), acquired via a high-frequency data management (HFDM) system at 100 Hz.
- Meteorological measurements at Mast 1 at 20 Hz: wind speed and direction at hub height, wind speed at 10 m height, air temperature, atmospheric pressure, and relative humidity at hub height.

2.2 Sound Immission Measurement

A long-term unsupervised sound immission measurement campaign was conducted from 1 March to 31 March 2025 using an outdoor sound monitoring station (IEC 60651, IEC 61672 class 1). A 1/2-inch microphone, equipped with a foam windscreen, was mounted at Mast 1 at a height of 2.8 m above ground. A-weighted equivalent sound pressure levels (L_{Aeq}) and 1/3 octave band spectra were recorded at a sampling interval of 0.1 seconds. No audio recordings were stored to ensure data privacy and reduce storage. A weather station located adjacent to the sound monitoring station at 2 m height provided concurrent meteorological data, i.e., air temperature, relative humidity, and wind speed. Post-processing procedures of the sound immission data are detailed in Section 3.

2.3 Sound Emission Measurement

A short-term sound emission measurement campaign was conducted on 19 February 2025 using twelve GPS-synchronised microphones positioned at 30° intervals and 100 m from OPUS 2. The reduced distance—compared to the IEC 61400-11:2012 [5] standard of $H + D/2 = 150$ m—was chosen to enhance SNR. Each acoustic measurement unit consists of a 1/2-inch microphone covered by a foam windscreen, mounted on a 1 cm thick wooden plate with a diameter of 1 m, ensuring compliance with IEC 61400-11:2012 [5] for ground reflection conditions.

During the campaign (9:45 UTC to 12:00 UTC), OPUS 1 was stopped, while OPUS 2 operated until 11:00 UTC, after which it was stopped for background sound measurement. A 2-minute segment under steady atmospheric and turbine operating conditions was selected for analysis. The measured time-series acoustic signals had a temporal resolution of 43 microseconds and were post-processed via a short-time Fourier transform (STFT) with a Hann window and 50 % overlap, yielding a frequency resolution of 11.71 Hz. Narrowband spectra were further processed to obtain A-weighted 1/3 octave band spectra (L) with centre frequencies ranging from 20 Hz to 10 kHz.

Immission-related sound power levels (L_{WA}) were determined using the formula:

$$L_{\mathrm{WA}} = \mathrm{L} - 6 + 10\, log\left(\frac{4\pi R^2}{S_0}\right) \tag{1}$$

where R is the oblique distance from the rotor centre to the microphone (in meters), and $\mathrm{S}_0 = 1\ \mathrm{m}^2$ is the reference area. The constant of 6 dB accounts for the approximate doubling of sound pressure level (SPL) observed during measurements on a rigid, acoustically hard plate. During the campaign, the HFDM system was unavailable; thus, the wind speed at hub height measured at Mast 1 was used for analysis.

A 6-minute segment free of human activity and other extraneous ambient noise was selected from the turbine-off background measurement. The SNR, defined as the ratio of SPL with the wind turbine operating to that with the turbine off, exceeds 10 dB across the frequency range of 200 Hz to 7000 Hz. This SNR level confirms adequate signal fidelity for reliable analysis of the wind turbine's acoustic emissions. Detailed post-processing procedures are documented in reference [7, 8] and are not repeated here for conciseness.

3 Data Processing and Analysis

3.1 Data Categorization

Sound immission data were aggregated into 1-minute intervals. The mean value (logarithmic mean for acoustic measurements and arithmetic mean for non-acoustic measurements) of each 1-minute interval was tagged by a timestamp corresponding to the beginning of the interval. All data across different data acquisition systems were paired by timestamp, forming a unified database.

The database includes only data corresponding to four turbine operation conditions:

- *OPUS 1 Only*: Only OPUS 1 operates and OPUS 2 is stopped.
- *OPUS 2 Only*: Only OPUS 2 operates and OPUS 1 is stopped.
- *Both Running*: Both wind turbines operate.
- *Both Stopped*: Both wind turbines are stopped.

Intermediate statuses (e.g., running up, shutting down, free-run) were excluded. Rotor yaw misalignment was restricted to ±15° to ensure consistent directional alignment.

3.2 Data Reduction and Filtering

A standard data reduction routine was applied to exclude transient extraneous sound events such as vehicle pass-by, human or animal activity, or transient natural sounds. The following statistical descriptors were used, as recommended in IEC TS 61400-11-2:2024 [9] and by Öhlund and Larsson [10]:

- $L_5 - L_{95} \leq 4$ dB(A)
- $L_1 - L_{95} \leq 15$ dB(A)
- The A-weighted 1/3 octave band sound level from 800 Hz and above should contribute less than 1.5 dB to the total A-weighted sound level if the total sound level is above 25 dB.
- The free-field spreading from every turbine (treated as point sources) must contribute to a total SPL of 30 dB(A) or above at the immission point.

Here, L_n denotes the sound level exceeded for n % of the time. For example, L_{90} means the SPL is above L_{90} for 90 % of the time.

3.3 Amplitude Modulation (AM) Evaluation

The periodic swishing sound of wind turbines was analyzed systematically using a method adapted from IEC TS 61400-11-2:2024 [9], Section 13.6.2.3, with modifications for robustness and clarity. The procedure is as follows:

1. Band-pass filtering: A-weighted band-pass filtered time-series signals (1-minute samples) were computed for six frequency ranges:
   - 50 Hz to 200 Hz
   - 100 Hz to 400 Hz
   - 200 Hz to 800 Hz
   - 400 Hz to 1600 Hz
   - 800 Hz to 3200 Hz
   - 1600 Hz to 6400 Hz

   The A-weighted overall sound pressure level (OASPL) was also analyzed.
2. Detrending: The time-series signal was detrended using a third-order polynomial least-squares fit (blue lines in Figure 1 (b) and Figure 2 (b)).
3. Discrete Fourier Transform (DFT): The detrended signal was transformed using DFT with a rectangular window and no data padding. The power spectrum S_{xx} was computed from the DFT output $F\{x\}$ as:

   $$\mathrm{S_{xx}} = \frac{|\mathrm{F}\{\mathrm{x}\}|^2}{\mathrm{m}^2} \tag{2}$$

   where $m = 600$ (number of samples).
4. Fundamental Frequency Detection: The fundamental frequency of modulation (i.e., the first harmonic frequency, f_1) was identified as the peak with the highest amplitude. It must agree with the blade passage frequency (BPF) within $\pm 3\Delta f/2$, where $\Delta f = 0.0167$ Hz. BPF is three times the mean rotor speed measured. If no such peak is found, the 1-minute sample is marked as "prominence-failed" and excluded.
5. AM Prominence Check:
   (a) Prominence ratio $p_{\mathrm{AM}} = L_{\mathrm{pk}}/L_{\mathrm{m}} \geq 4$, where L_{pk} is the amplitude at f_1 in S_{xx}, and L_{m} is the average amplitude of two spectral lines on either side of the peak (excluding adjacent lines).

   (b) The peak-to-peak amplitude of the time-series generated by inverse transform using only the energy at f_1 must be > 1.5 dB.

   If either condition fails, the sample is marked as "prominence-failed".
6. Harmonic Inclusion:
   (a) Check for local maxima within N lines on either side of the 2nd and 3rd harmonics (at $2f_1$ and $3f_1$), where $N = 1$ for the 2nd harmonic and $N = 2$ for the 3rd.

   (b) Include the harmonic in the inverse transform only if its peak-to-peak amplitude > 1.5 dB.
7. Reconstruction: Inverse Fourier transform was applied to the fundamental and selected harmonics (three lines at each), yielding a time series resembling the original but containing only energy related to the identified frequencies (orange lines in Figure 1 (a) and Figure 2 (a)).
8. Modulation Depth: Calculated as $L_5 - L_{95}$ of the reconstructed time series.

Figure 1 and Figure 2 illustrate the AM analysis workflow for two band-pass frequency ranges and two different operational conditions. It is worth noting that in Figure 2, the second and third harmonics were not included due to low peak-to-peak amplitudes, resulting in a lower AM depth than visually apparent. Further fine-tuning of p_{AM} and peak-to-peak thresholds may be needed if higher harmonics are of interest, but this is beyond the scope of this study.

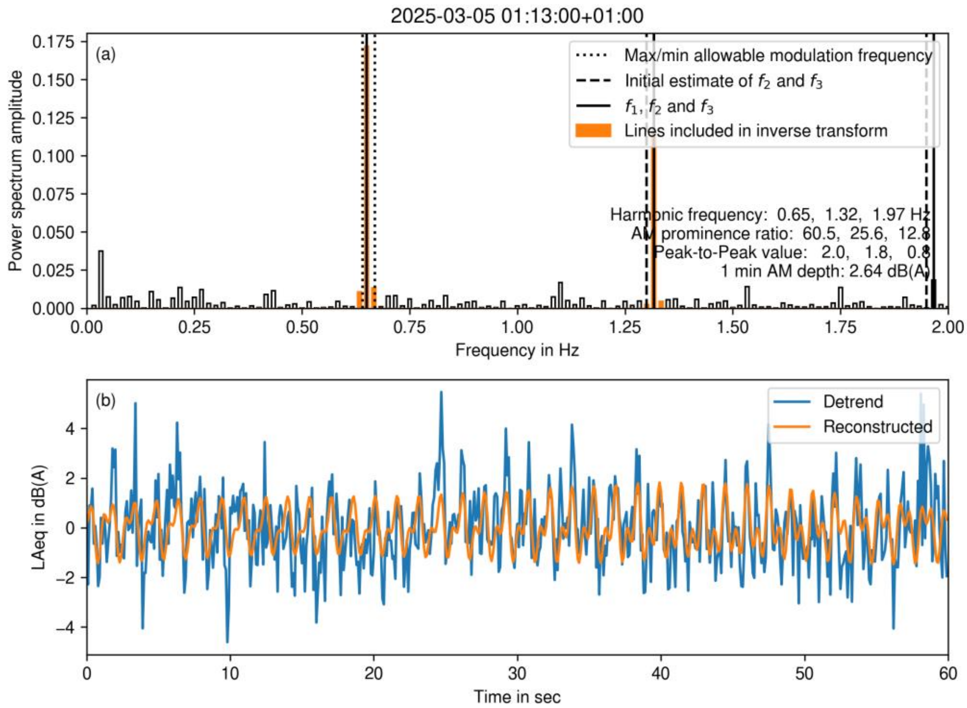

Figure 1: AM analysis workflow: (a) Power spectrum; (b) Detrended and reconstructed time series (Band-pass frequency range: 50 Hz to 200 Hz)

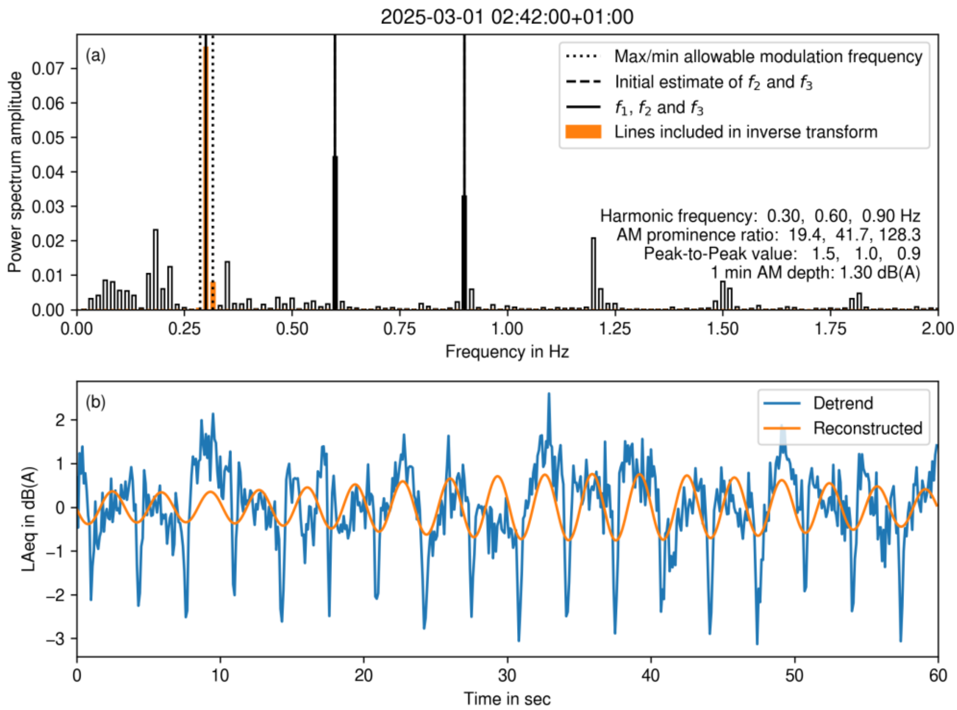

Figure 2: AM analysis workflow: (a) Power spectrum; (b) Detrended and reconstructed time series (Band-pass frequency range: 1600 Hz to 6400 Hz)

4 Results and Discussion

4.1 Data Binning and Selection

Sound immission measurements were binned by turbine operational wind speed, which was determined from the turbine's power curve with a tolerance of $P_{\mathrm{tol}} = 1\ \%$, following IEC 61400-11:2012 [5]:

$$(P_{k+1} - P_{\mathrm{tol}}) - (P_k + P_{\mathrm{tol}}) > 0 \tag{3}$$

where k is the wind speed bin index and P_k is the power curve value at bin k. Generator mechanical power from the HFDM was calibrated using a one-dimensional polynomial fit derived from linear regression between SCADA electric power and measured mechanical power during the campaign. A manufacturer-provided power curve was used as reference. Data outside the power curve range (Equation (3)) were excluded. Figure 3 (a) depicts the measurements across a wide range of wind speed from 4 m/s to 12 m/s.

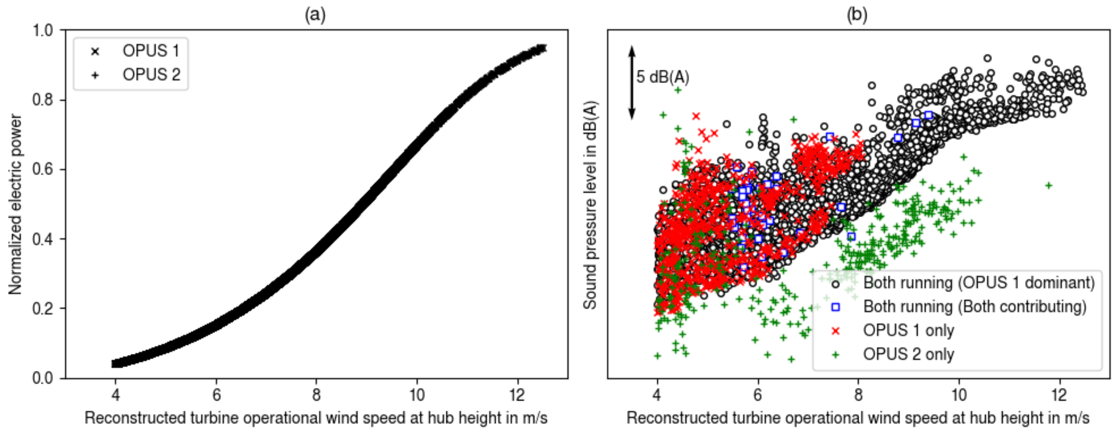

Figure 3: (a) Normalized electric power vs. turbine operational wind speed; (b) Measured SPL by turbine status

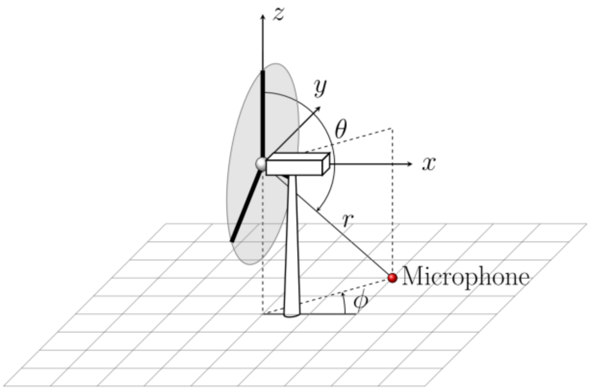

Figure 4: Microphone azimuth ϕ definition relative to turbine axis

When only one turbine operated, data were binned by the operational wind speed of that turbine (Figure 3 (b)). For simultaneous operation, the turbine wind speed, following IEC TS 61400-11-2:2024 [9] Section 9.3.2.3, was either:

- the mean wind speed if both turbines contributed similarly, or
- the wind speed of the dominant turbine.

Data were further binned according to the azimuth angle ϕ, defined as the angular position around the turbine tower axis, measured counter-clockwise from the downwind direction (Figure 4). Specifically, $\phi = 0°$ corresponds to the downwind microphone position, $\phi = 180°$ to the upwind position, $\phi = 90°$ to the crosswind direction with the rotor blade moving upward, and $\phi = 270°$ to the crosswind direction with the blade moving downward. In practice, the rotor yaw is assumed to be perfectly aligned with the wind direction, so the azimuth angle is determined directly from the wind direction.

Figure 5 presents the data distribution across wind speed and azimuth bins, with the count of data points in each bin. Most data fall in upwind and downwind positions due to turbine alignment with the prevailing wind direction. Crosswind data are sparse, limiting full directional characterization.

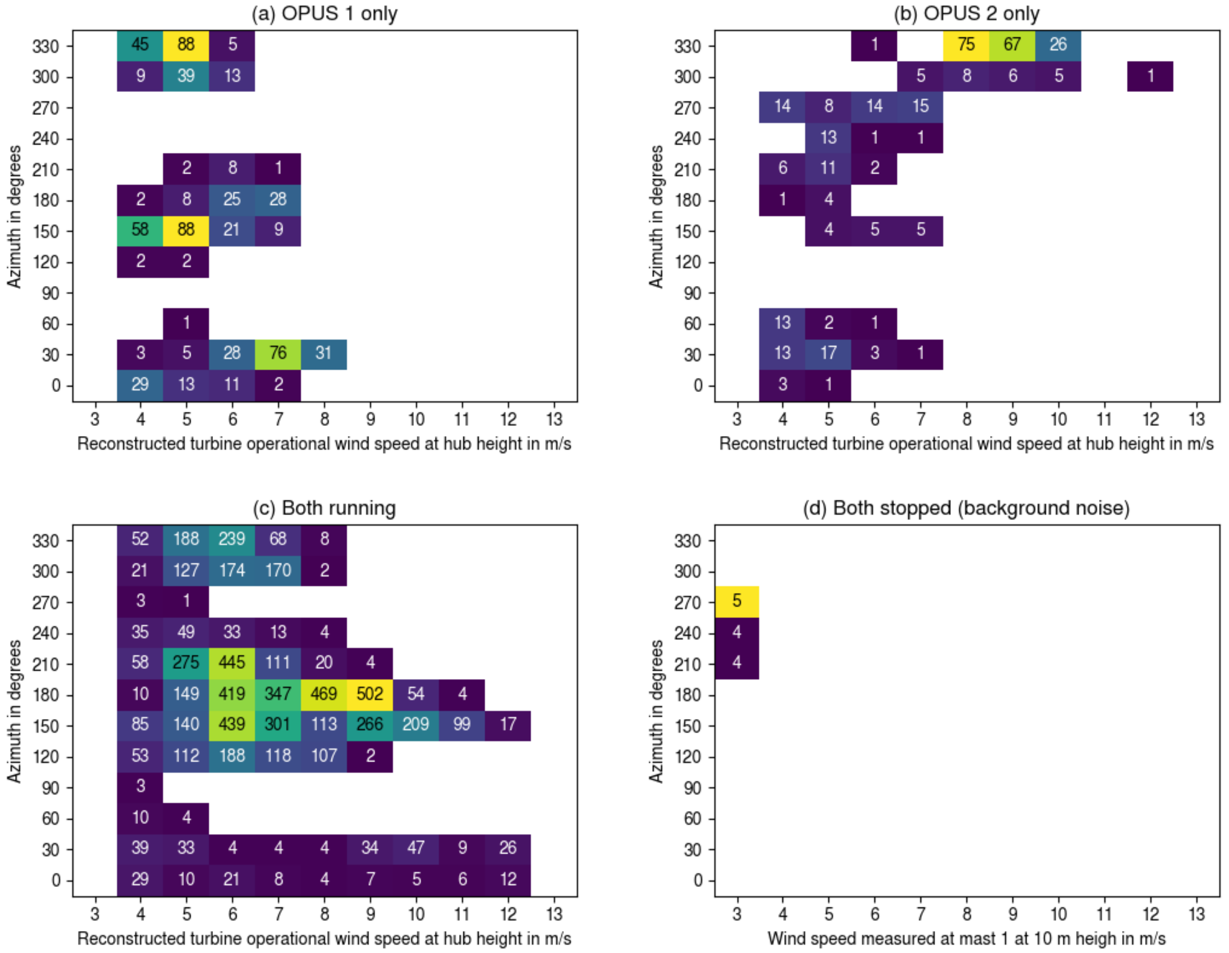

Figure 5: Wind speed and azimuth bin distribution with corresponding data counts

4.2 Wind-Induced Noise and Data Filtering

Open-field acoustic measurements are inherently susceptible to wind-induced noise, including two primary components: microphone self-noise (dominant at low frequencies) and wind-induced vegetation noise (dominant at high frequencies) [10]. Both sources exhibit a strong dependence on wind speed at microphone height and can be systematically mitigated through appropriate data filtering strategies.

Table 1: Data filtering: Criterion A

Quality	Measured/Derived	Binning/Filtering	Range of interest
Turbine operational wind speed	Derived	Binning	$\geq 7.5\ \mathrm{m/s}$
Wind speed at microphone	Measured	Filtering	$< 3\ \mathrm{m/s}$

Empirical analysis reveals a monotonic increase in measured SPLs with increasing wind speed at the microphone (Figure 6). To determine whether this increase is attributable to microphone self-noise, the manufacturer-provided specification for wind-induced self-noise at a microphone wind speed of 5 m/s is also plotted in Figure 6 (dotted lines). The measured

SPLs significantly exceed the self-noise contribution across a wide wind speed range, indicating that the observed rise in noise levels is not due to microphone self-noise but rather to ambient wind-induced noise from the surrounding environment. This conclusion holds regardless of the source of the extraneous noise, whether from turbulent flow over the microphone windscreen, vegetation, or ground-level turbulence. To minimize contamination from wind-induced ambient noise, a wind speed threshold of less than $3\,\mathrm{m/s}$ at microphone height is applied in conjunction with the operational wind speed range of interest ($\geq 7.5\,\mathrm{m/s}$), forming a wind speed-based data filtering criterion, Criterion A (Table 1). This filtering criterion effectively reduces data scattering within each wind speed bin, as illustrated in Figure 7 (a), resulting in a more reliable dataset.

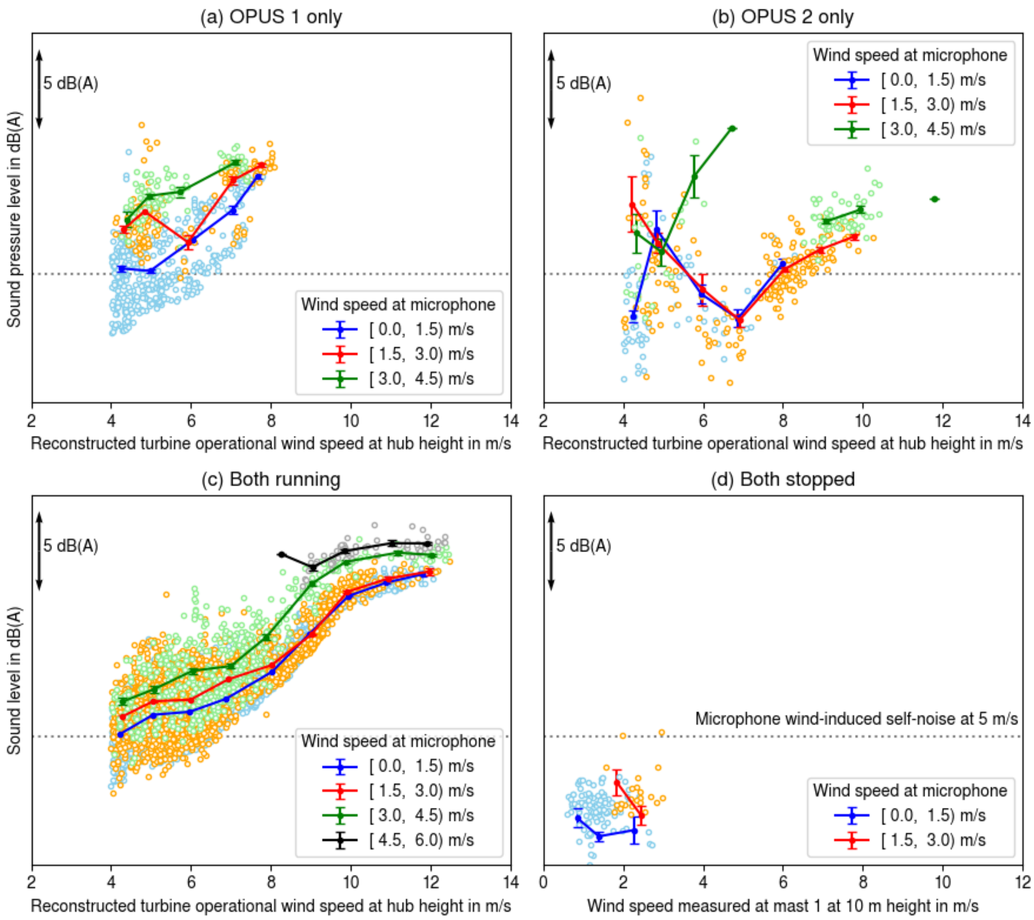

Figure 6: Influence of wind speed at microphone on SPLs

While restricting the wind speed at the microphone efficiently excludes highly contaminated data, it is not inherently sensitive to turbine-generated sound. Therefore, to ensure objective identification of wind turbine sound emissions, we adopt a procedure similar to [11], leveraging the natural, periodic AM characteristic of wind turbine noise, the so-called swishing sound, associated with the BPF. A signal is classified as turbine-generated sound only if its AM exhibits sufficient prominence (see Section 3.3).

Table 2 shows the detection rate of wind turbine sound across the six band-pass frequency ranges and the OASPL. The detection rate decreases monotonically with increasing wind speed at the microphone. Notably, at wind speeds exceeding 3 m/s, the detection rate drops to near zero, confirming that turbine sound is effectively masked by ambient noise under these conditions. Given that the 50–200 Hz band yields the highest detection rate, this frequency range is selected as the primary band for AM-based signal identification.

Combined with the AM prominence criterion, a second data filtering criterion, Criterion B (Table 3), is established. This dual-filtering approach further reduces data variability, as shown in Figure 7 (b). The resulting dataset includes only measurements corresponding to:

- *OPUS 1 Only*: OPUS 1 operating, OPUS 2 stopped, and

- *Both Running (OPUS 1 dominant)*: Both turbines operate, but OPUS 1 dominates the acoustic contribution.

No data from *OPUS 2 Only* or *Both Running (both contributing)* remain. This absence is consistent with the greater distance between OPUS 2 and the sound monitoring station, resulting in a significantly lower SPL and higher susceptibility to ambient noise. Consequently, the acoustic signature of OPUS 2 is undetectable under the current filtering criteria.

Table 2: Detection rate of wind turbine sound by AM prominence (*Both Running with OPUS 1 dominant* and turbine operational wind speed $\geq 7.5\ \mathrm{m/s}$)

Wind speed at microphone	0–1.5 m/s	1.5–3 m/s	3–4.5 m/s	4.5–6 m/s
Sample count	1132	675	155	69
OASPL	6.5 %	11.6 %	5.29 %	0 %
50–200 Hz	34.9 %	29.8 %	7.1 %	2.9 %
100–400 Hz	10.1 %	6.7 %	0 %	0 %
200–800 Hz	4.8 %	3.7 %	0 %	0 %
400–1600 Hz	4.5 %	1.9 %	0 %	0 %
800–3200 Hz	5.6 %	4.7 %	1.3 %	0 %
1600–6400 Hz	6.5 %	11.6 %	5.2 %	0 %

Table 3: Data filtering: Criterion B

Quality	Measured/Derived	Binning/Filtering	Range of interest
Turbine operational wind speed[1]	Derived	Binning	$\geq 7.5\ \mathrm{m/s}$
Wind speed at microphone	Measured	Filtering	$< 3\ \mathrm{m/s}$
AM prominence[2]	Derived	Filtering	Prominent

[1]When both wind turbines operate, data representing *OPUS 1 dominant* are considered.

[2]Unless otherwise specified or explicitly notified, the band-pass frequency range of 50–200 Hz is applied.

Since both *OPUS 1 Only* and *Both Running (OPUS 1 dominant)* represent the acoustic emission of OPUS 1 under varying operational conditions, they are merged for subsequent analysis. The unified dataset is thus representative of OPUS 1's sound immission under real-world, variable meteorological conditions, with minimal contamination from ambient noise.

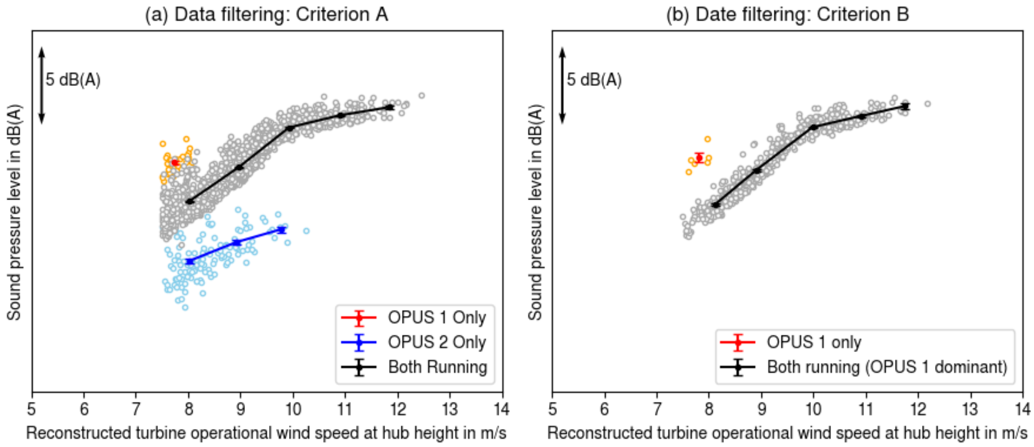

Figure 7: Filtered sound levels using (a) Criterion A and (b) Criterion B

4.3 Directional and Meteorological Influences on Sound Immission

Following the application of rigorous noise filtering (Section 4.2), the remaining dataset consists of high-fidelity sound immission measurements representative of wind turbine emissions. This filtered data enables a meaningful analysis of directional and meteorological dependencies on sound propagation.

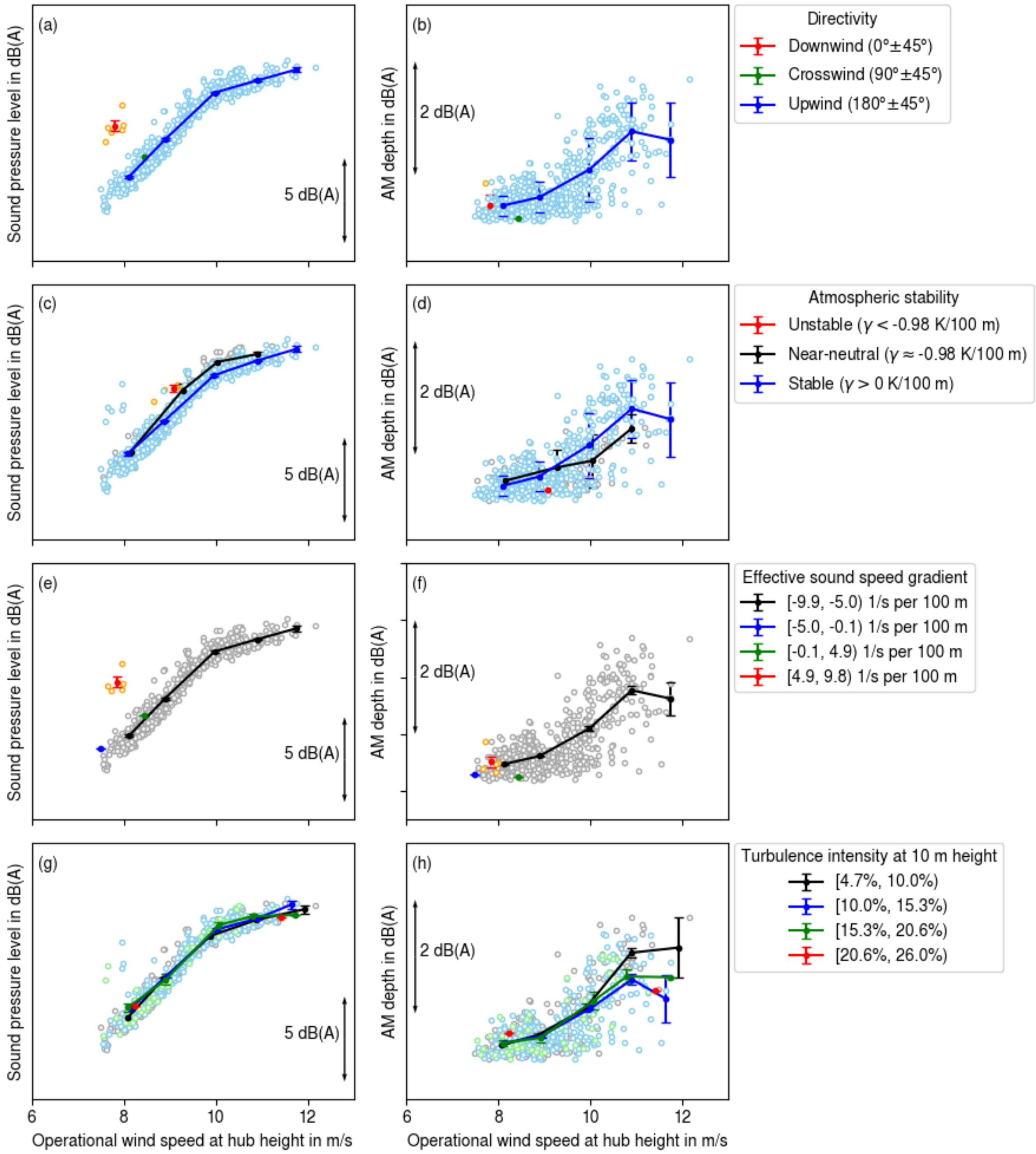

Figure 8: Influence of directivity and meteorology on sound levels and AM depth (Criterion B, band-pass frequency range: 50–200 Hz)

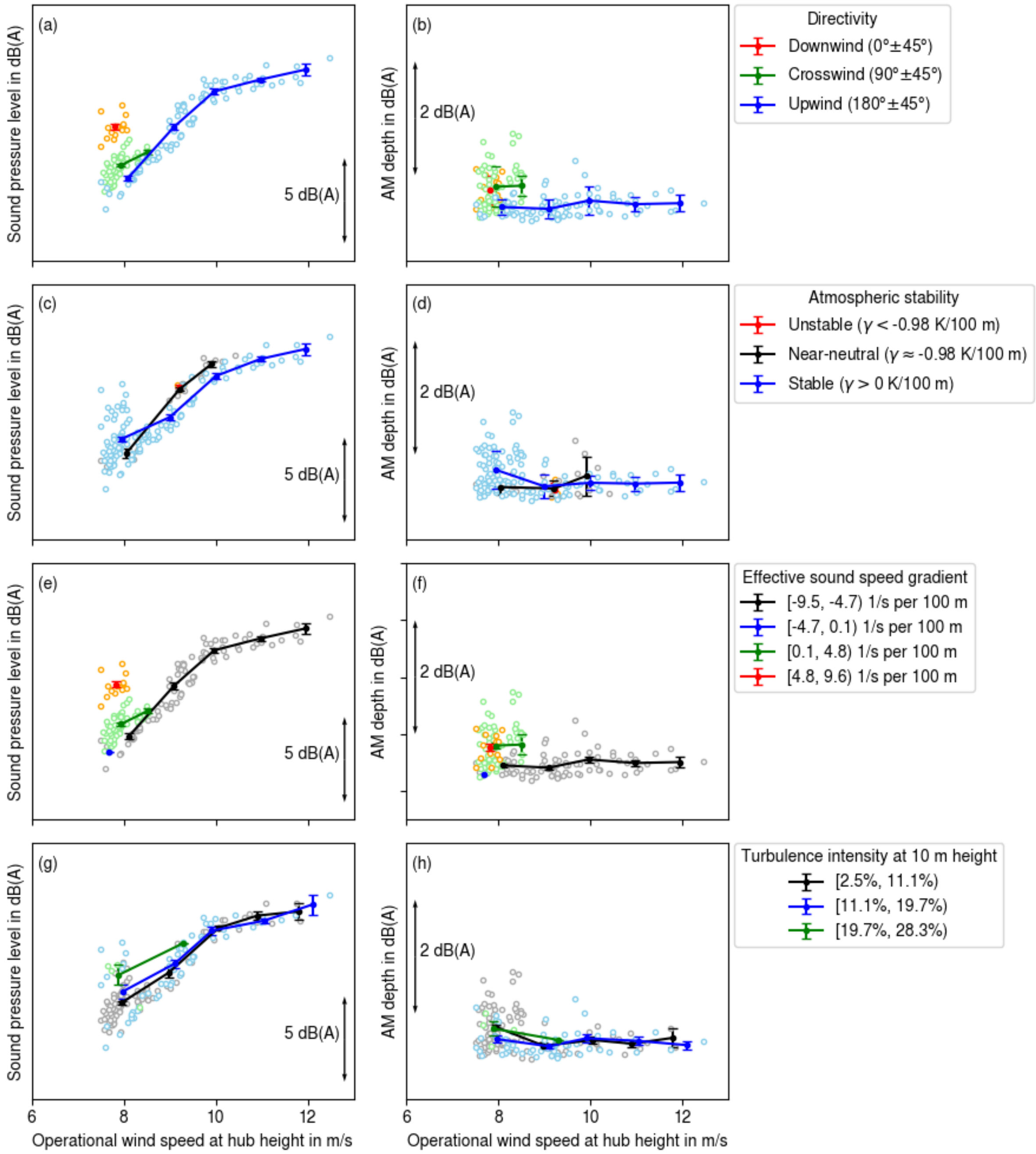

Figure 9: Influence of directivity and meteorology on sound levels and AM depth (Criterion B, band-pass frequency range: 1600–6400 Hz)

4.3.1 Directional Distribution and Downwind Bias

The directional distribution of the filtered data is illustrated in Figure 8 (a). The majority of measurements correspond to the upwind configuration, while data in the downwind and crosswind directions are sparse. The scarcity of crosswind data is attributable to the limited availability of such configurations in the initial dataset, consistent with the prevailing wind direction at WiValdi. Notably, near all downwind measurements were excluded during filtering, primarily due to elevated ambient noise levels. This phenomenon is readily explained by the presence of accelerated flow below the turbine wake (see Figure 3 in [12]), which enhances wind-induced turbulence and ambient noise at microphone height. This significantly degrades the SNR in the downwind direction, precisely the configuration of greatest interest for regulatory and community impact assessments. Thus, the observed data scarcity in the downwind sector reflects both physical limitations and the challenges inherent in acquiring high-quality acoustic data under such conditions.

4.3.2 Directional Sound Level Variation and Discrepancy with Predictions

Figure 8 (a) shows that, at the turbine operation wind speed of 8 m/s, sound levels in the downwind position are significantly higher than those in the upwind position. A similar trend is observed in Figure 11 (a) (cross symbols), where SPLs are predicted from the sound power level (L_{WA}) derived from the concurrent emission campaign:

$$\mathrm{L} = \mathrm{L_{WA}} - 10\log(4\pi \mathrm{R}^2) \tag{4}$$

where R is the oblique distance from the rotor centre to the monitoring station position. While the overall trend between measured and predicted levels is consistent, the magnitude of the upwind-downwind difference in the immission data is substantially larger than in the prediction. To resolve this discrepancy, a comparative analysis of 1/3 octave band spectra was conducted. The emission spectra (Figure 11 (b)) exhibit near-identical shapes across all azimuthal directions, indicating that the source characteristics are directionally invariant. In contrast, the immission spectra (Figure 10 (a)) show pronounced directional differences, particularly in the 20–100 Hz and 400–2000 Hz ranges.

To further investigate, the logarithmic mean of the immission spectra in the 9 m/s wind speed bin was compared with a corrected prediction:

$$\mathrm{L} = \mathrm{L_{WA}} - 10\log(4\pi \mathrm{R}^2) + \mathrm{m} \times 10\log\left(\frac{\mathrm{V_2}}{\mathrm{V_1}}\right) \tag{5}$$

where $m = 2.64$ is empirically derived from the immission data (Figure 12 (a)); V_1 is the wind speed during the emission campaign, and V_2 is the mean wind speed in the 9 m/s bin. The correction accounts for wind speed variation affecting sound emission. The predicted spectrum shows good agreement with the measured data in frequency bands above 500 Hz (Figure 12(b)). However, a notable discrepancy is observed at frequencies below 500 Hz. Despite this deviation, the detection rate of wind turbine sound amplitude modulation in the 50–200 Hz range remains higher than in other frequency bands (Table 2), suggesting that the underlying modulation characteristics are still discernible.

The spectrum of wind-induced noise at the microphone, as specified by the manufacturer for a wind speed of 5 m/s, is also shown in Figure 12(b) (grey line). This value is significantly lower than the measured sound pressure levels, indicating that microphone self-noise is not the primary contributor to the observed discrepancy. The mismatch in the low- and mid-frequency ranges is therefore likely attributable to ground reflection effects and external sources of ambient noise, such as wind-induced vibrations on nearby structures—including mast booms, wires, and vegetations. Nevertheless, the consistent spectral characteristics observed between immission and emission measurements support the conclusion that the filtered dataset effectively captures turbine-generated sound, rather than being dominated by ambient interference.

Sound levels increase approximately linearly with turbine operational wind speed (Figure 8 (a)). However, above 10 m/s, the rate of increase begins to diminish, consistent with the rotor reaching its rated speed and the onset of blade pitch control. This transition is further supported by the 1/3 octave spectra (Figure 10 (b)), which show a marked convergence at higher wind speeds. The narrowing of spectral variation indicates that the acoustic signature becomes increasingly stable and less sensitive to small fluctuations in wind speed.

The AM depth in the 50–200 Hz band exhibits a clear increase with turbine operational wind speed (Figure 8 (b)). In contrast, no such trend is observed in the 1600–6400 Hz band (Figure 9 (b)), where the AM depth remains relatively constant across wind speeds. This behaviour is attributed to the neglect of higher harmonics in the inverse Fourier transform, as discussed in Section 3.3, which introduces an artificial suppression of modulation effects at higher frequencies.

4.3.3 Influence of Atmospheric Stability

Given the relatively short source-receiver distance (250 m from the OPUS 1 rotor centre to the monitoring station), direct effects of atmospheric absorption and refraction are expected to be minimal. Figure 8 (c) and (d) illustrate the variation in sound levels and AM depth with atmospheric stability γ, defined as the vertical temperature gradient derived from measurements at hub height and at 2 m height. Unstable stratification is associated with slightly higher sound levels, while stable stratification (temperature inversion) correlates with increased AM depth at high wind speeds. This trend is counterintuitive in light of classical atmospheric acoustics, which predicts that stable stratification enhances sound propagation through downward refraction, thereby increasing received sound levels near the ground. The observed decrease in sound levels under stable conditions thus contradicts this expectation. This discrepancy suggests that propagation effects may be overshadowed by other dominant factors, particularly the wind shear. To better interpret the observed behavior, both the temperature gradient and wind shear must be considered jointly, as they jointly influence the effective sound speed gradient and consequently sound refraction patterns.

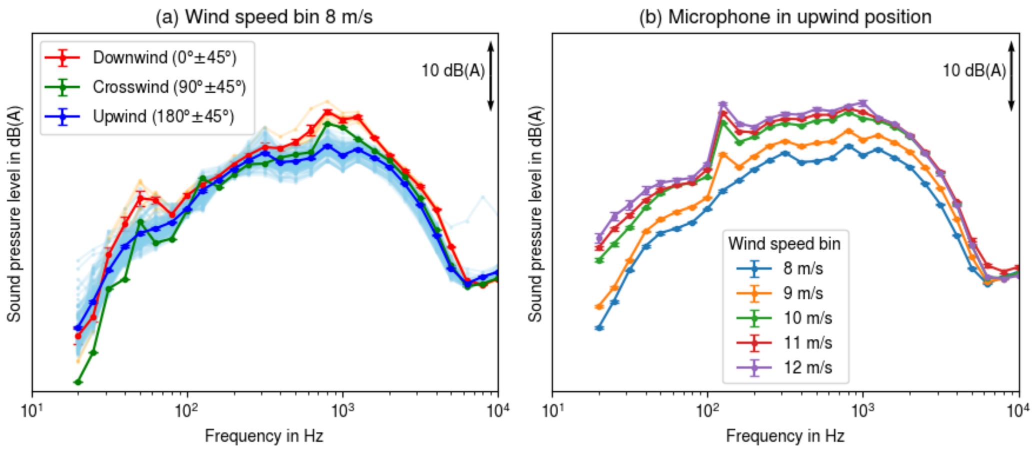

Figure 10: Influence of (a) directivity and (b) operational wind speed on 1/3 octave spectra

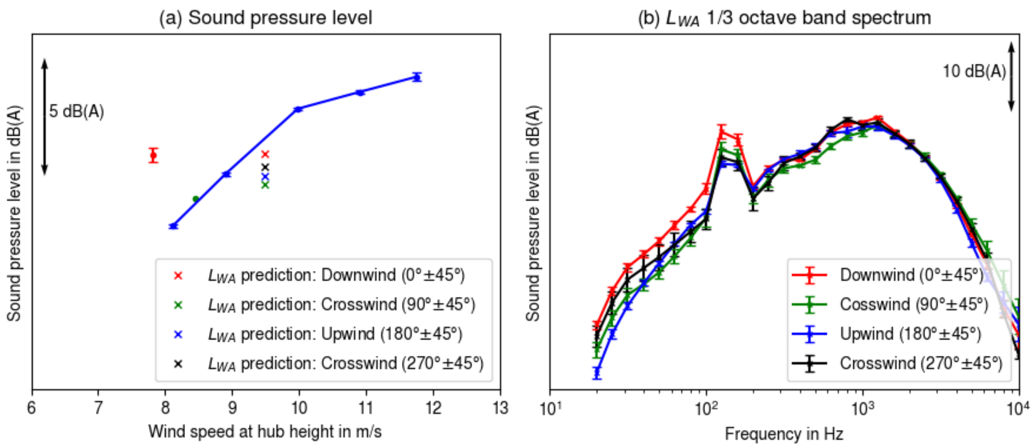

Figure 11: (a) Comparison of sound immission levels with predictions; (b) 1/3 octave band spectra of the emission campaign

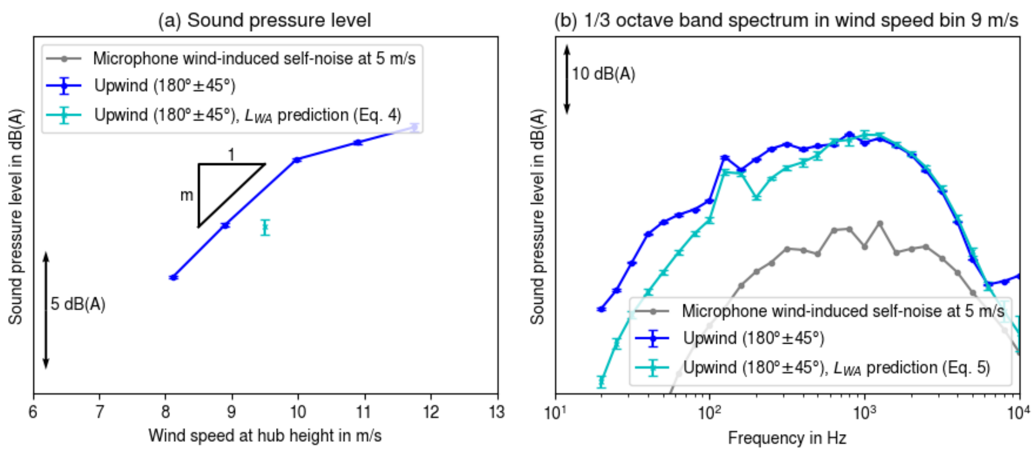

Figure 12: Comparison of the sound immission levels to predictions: (a) SPLs; (b) 1/3 octave band spectra

4.3.4 Effect of Effective Sound Speed Gradient

The propagation of sound from elevated sources such as wind turbines is strongly influenced by atmospheric inhomogeneities, particularly vertical gradients in temperature and wind speed component in the propagation direction. To capture the combined effect of these two key factors, the vertical gradient of effective sound speed is employed as a unified metric. The effective sound speed is defined as:

$$c_{\mathrm{eff}} = \mathrm{c} + \mathrm{V}\, cos(\phi) \tag{6}$$

where c is the adiabatic speed of sound, V is the wind speed, and ϕ is the azimuth angle (Figure 4). The adiabatic speed of sound c is computed from air temperature and relative humidity [13]:

$$c = \sqrt{\gamma RT(1 + 0.16h)} \tag{7}$$

with γ as the specific heat ratio, R as the gas constant for dry air, air temperature T in Kelvin, and h as the dimensionless mole fraction of water vapor in air.

Positive effective sound speed gradients correspond to sound focusing through downward refraction, while negative gradients lead to de-focusing via upward refraction. This implies that sound levels in conditions of positive effective sound speed gradients will be higher than those with negative ones. The sound level measurements with positive sound speed gradients (red lines in Figure 8 (e) and Figure 9 (e)) are indeed much higher than those with negative sound speed gradients. However, these trends also align qualitatively with the observed directional patterns in Figure 8 (a) and Figure 9 (a). It is crucial to emphasize that the higher sound levels observed downwind, despite the presence of a positive effective sound speed gradient, do not necessarily imply a causal role of refraction. The wind turbine's aerodynamic noise emission is inherently directional, with significantly higher sound power radiated in the downwind direction (cross symbols in Figure 11 (a)). Therefore, the observed increase in sound levels downwind may be primarily attributed to this inherent emission directivity, rather than propagation effects. In this context, the influence of refraction may be secondary or even masked by the dominant emission pattern. Thus, while the effective sound speed gradient provides a useful framework for understanding propagation, its role in shaping the observed sound levels cannot be confirmed without accounting for the turbine's intrinsic directional emission characteristics.

The AM depth has no significant dependency with respect to the sound speed gradient (Figure 8 (f) and Figure 9 (f)).

4.3.5 Turbulence Intensity Effects

The influence of turbulence intensity, derived from wind speed measurements at 10 m height at Mast 1, is also examined (Figure 8 (g) and (h), and Figure 9 (g) and (h)). Within the range of 5 % to 26 % available, no discernible effect on sound levels or AM depth is observed. This suggests that, under the current conditions, turbulence intensity alone does not significantly modulate the observed acoustic features, although its role in long-range propagation may still be relevant.

5 Conclusions and Outlook

This study demonstrates the feasibility of using a single, permanent sound monitoring station to accurately characterize wind turbine sound immission under real-world conditions, capturing directional dependencies and AM patterns with high fidelity. Despite the limitations of a single-station setup, the final dataset, filtered via AM prominence and wind speed criteria, shows strong agreement with high-SNR reference measurements from a concurrent short-term emission campaign, validating the proposed data filtering approach for low SNR sound immission measurements.

Key findings include:

- Clear AM at the BPF is observed, with greater modulation depth under higher turbine loads.
- Significant directional and spectral variability in sound levels is evident in both campaigns.
- Wind speed at microphone height, linked to high sound levels and low AM prominence, is as a critical confounder, especially for downwind observers.
- Meteorological effects on sound propagation are minimal over short distances.

The primary limitation remains the lack of crosswind data and the inability to resolve true directivity due to the single-station configuration.

Outlook: A follow-up study is underway, deploying a multi-station array at WiValdi. This will enable:

- High-fidelity mapping of sound directivity

- Quantification of propagation effects (e.g., ground reflection, refraction, wake interference)
- Validation of low-noise blade designs and noise mitigation strategies.

These efforts will advance the scientific basis for wind turbine noise regulation and community engagement, supporting the sustainable expansion of wind energy.

References

[1] C. H. Hansen, C. J. Doolan und K. L. Hansen, Wind Farm Noise: Measurement, Assessment, Wiley, 2017.

[2] H. H. Hubbard und K. P. Shepherd, „Wind turbine acoustics," NASA Technical Paper 3057; DOE/NASA/20320-77, 1990.

[3] S. Oerlemans, „Nlr-Tp-2011-066," 2011.

[4] S. Wagner, R. Bareiß und G. Guidati, Wind Turbine Noise, Springer, 1996.

[5] IEC 61400-11:2012, Wind turbines - Part 11: Acoustic noise measurement techniques.

[6] G. P. van den Berg, „Effects of the wind profile at night on wind turbine sound," *Journal of Sound and Vibration,* pp. 955-970, 2004.

[7] A. Suryadi, P. Seelemeyer, H. Bucholz, S.-M. Pott-Pollenske, C. Appel, S.-Y. Lin und M. Herr, „Sound Directivity Measurement at The WiValdi Research Wind Park," in *22. STAB-Workshop*, 2025.

[8] P. Seelemeyer, A. Suryadi, H. Buchholz, M. Pott-Pollenske und S.-Y. L. M. H. Christina Appel, „Sound Directivity Measurement at The WiValdi Research Wind Park," in *DAGA*, Dresden, 2026.

[9] IEC TS 61400-11-2:2024, Wind energy generation systems - Part 11-2: Acoustic noise measurement techniques – Measurement of wind turbine sound characteristics in receptor position.

[10] O. Öhlund und C. Larsson, „Meteorological effects on wind turbine sound propagation," *Applied Acoustics,* pp. 34-41, 2015.

[11] A. Schady und K. Elsen, „On the detectability of wind turbine noise under different meteorological conditions," in *Proceedings of Meetings on Acoustics*, 2020.

[12] D. Heimann, „Modelling sound propagation from a wind turbine under various atmospheric conditions," *Meteorologische Zeitschrift,* pp. 265-275, 2018.

[13] E. M. Salomons, Computational Atmospheric Acoustics, Springer, 2001.